

Volumetric breast density evaluation from ultrasound tomography images

Carri K. Glide-Hurst^{a)}

William Beaumont Hospital, 3601 West Thirteen Mile Road, Royal Oak, Michigan 48073

Neb Duric and Peter Littrup

Karmanos Cancer Institute, Hudson-Webber Cancer Research Center, 110 East Warren, Room 5040, Detroit, Michigan 48201

(Received 19 November 2007; revised 2 July 2008; accepted for publication 2 July 2008; published 11 August 2008)

Previous ultrasound tomography work conducted by our group showed a direct correlation between measured sound speed and physical density *in vitro*, and increased *in vivo* sound speed with increasing mammographic density, a known risk factor for breast cancer. Building on these empirical results, the purpose of this work was to explore a metric to quantify breast density using our ultrasound tomography sound speed images in a manner analogous to computer-assisted mammogram segmentation for breast density analysis. Therefore, volumetric ultrasound percent density (USPD) is determined by segmenting high sound speed areas from each tomogram using a k-means clustering routine, integrating these results over the entire volume of the breast, and dividing by whole-breast volume. First, a breast phantom comprised of fat inclusions embedded in fibroglandular tissue was scanned four times with both our ultrasound tomography clinical prototype (with 4 mm spatial resolution) and CT. The coronal transmission tomograms and CT images were analyzed using semiautomatic segmentation routines, and the integrated areas of the phantom's fat inclusions were compared between the four repeated scans. The average variability for inclusion segmentation was $\sim 7\%$ and $\sim 2\%$, respectively, and a close correlation was observed in the integrated areas between the two modalities. Next, a cohort of 93 patients was imaged, yielding volumetric coverage of the breast (45–75 sound speed tomograms/patient). The association of USPD with mammographic percent density (MPD) was evaluated using two measures: (1) qualitative, as determined by a radiologist's visual assessment using BI-RADS Criteria and (2) quantitative, via digitization and semiautomatic segmentation of craniocaudal and mediolateral oblique mammograms. A strong positive association between BI-RADS category and USPD was demonstrated [Spearman $\rho=0.69$ ($p < 0.001$)], with significant differences between all BI-RADS categories as assessed by one-way ANOVA and Scheffé posthoc analysis. Furthermore, comparing USPD to calculated mammographic density yielded moderate to strong positive associations for CC and MLO views ($r^2=0.75$ and 0.59 , respectively). These results support the hypothesis that utilizing USPD as an analogue to mammographic breast density is feasible, providing a nonionizing, whole-breast analysis. © 2008 American Association of Physicists in Medicine. [DOI: 10.1118/1.2964092]

Key words: breast density, ultrasound tomography, mammographic percent density, sound speed

I. INTRODUCTION

Emerging evidence has shown that women with high mammographic breast density are at four to five-fold increased risk of developing breast cancer.^{1–4} The appearance of breasts in mammograms varies due to differences in the amount of fat, connective, and epithelial tissues present.⁵ Fibroglandular and connective tissues (i.e., glands, ducts, and fibers) have high x-ray attenuation, rendering them radiologically dense and appearing light on radiographic films. By contrast, fat appears radiolucent, or dark, on a processed film. Because of the distinct differences in x-ray attenuation between fat and fibroglandular tissue, segmentation of fibroglandular tissue from the rest of the breast is possible. Thus, mammographic percent density (MPD) can be calculated as the ratio of fibroglandular tissue area divided by the total breast area. Increased MPD has proven to be more prognostic of overall breast cancer risk than nearly all other risk

factors.^{6–9} Further, having elevated breast density is fairly common; research has shown $\sim 25\%$ of all women exhibit dense breasts,⁵ while up to $\sim 40\%$ of women in their forties show evidence of this trait.⁸ By contrast, an estimated 2%–10% of women exhibit the two breast cancer susceptibility genes, BRCA1 and BRCA2.^{10–13} These data suggest that women with breast cancer attributable to increased breast density are likely to form a significant percentage of overall breast cancer cases, and as a result, finding new techniques to quantify breast density is particularly advantageous.

Perhaps the most remarkable characteristic of breast density is the fact that it can be modified. This is significant because many contributing factors for breast cancer risk (i.e., age, family history) cannot be changed. Because breast density *can* be altered, it has been suggested for use as a surrogate marker,¹⁴ intermediate phenotype for breast cancer,¹⁵ and indicator for monitoring potential preventive^{16,17} or

therapeutic strategies.^{18–22} Hormones play an integral role in breast density change; Tamoxifen^{18,23} and other chemopreventative agents such as soy isoflavones have been shown to decrease breast density.^{24–26} Furthermore, identifying women with elevated breast cancer risk due in part to increased breast density may better enable preventive measures (i.e., more frequent screening or chemopreventative agents) that have the potential to reduce breast cancer incidence.

However, the standard of care in breast density evaluation currently involves radiologists' visual assessment of mammograms using the four-category Breast Imaging Reporting and Data System (BI-RADS) lexicon. This subjective classification has proven to be limited due to considerable intra- and interreader variability.^{27,28} Several groups have also estimated quantitative breast density from digitized film-screen or digital mammograms via computer-assisted segmentation routines.^{29–32} While these approaches have proven to be more accurate for breast density evaluation, digitizing mammograms is cumbersome and time consuming, thereby making it impractical to carry out larger studies. While digital mammography eliminates the need for digitization, mammographic breast density estimates were found to be significantly lower using digital mammography—due to more subcutaneous fat being included near the skin/background boundary—than in film-screen mammography.³³ This implicitly suggests that breast cancer risk assessment would, in turn, be underestimated when measured with digital mammography. Regardless of the images being digital or film-screen, mammograms, by definition, both still represent a 2D projection that cannot provide an accurate volumetric estimate of the density due to the breast thickness not being taken into account.

Most likely, breast cancer risk would be more strongly related to the *volume* of dense tissue as opposed to the projected area. To this end, efforts have been made to estimate volumetric breast density through computational modeling,^{34,35} evaluating whole-breast MRI sequences,^{36,37} and calibrating screen-film images with step wedges.³² The volumetric measure that we are presenting, however, is novel due to using ultrasound tomography transmission images (i.e., sound speed) to provide estimates of volumetric breast density. Previous work conducted by our group showed a direct correlation between the measured sound speed and physical density of phantom inclusions.³⁸ We also demonstrated an increase in global breast sound speed with increasing mammographic density *in vivo*.³⁸ Building on these empirical results, the purpose of this work was to explore the quantification of breast density using our ultrasound tomography sound speed images in a manner analogous to computer-assisted mammographic percent density segmentation. Therefore, volumetric ultrasound percent density (USPD) is determined by segmenting high sound speed areas from each tomogram using a k-means clustering routine, integrating these results over the entire breast, and dividing by whole-breast integrated area as described in the Methods section. As an initial proof of concept, we demonstrate results from an anthropomorphic breast phantom experiment to directly compare segmented areas from both coronal CT im-

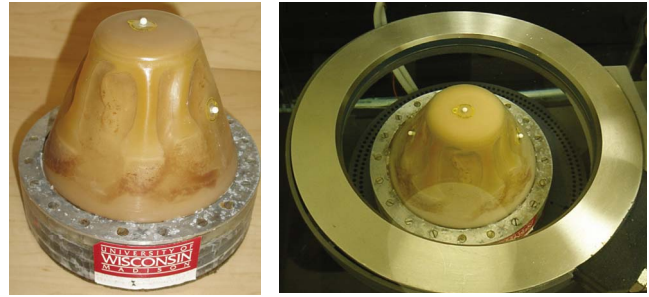


FIG. 1. Left: the breast phantom provides tissue-equivalent scanning characteristics with simulated fat inclusions embedded in fibroglandular tissue. Right: close up of the phantom surrounded by the transducer ring that translates in the z-direction to image the entire phantom volume.

ages and sound speed tomograms. Further, we present *in vivo* USPD results and evaluate them with two methods of breast density estimation: (1) the current standard of care (e.g., BI-RADS categories) and (2) quantitative breast density measurements obtained through calculated MPD.

II. METHODS AND MATERIALS

II.A. Breast phantom scanning procedure

All ultrasound tomography scans were performed with our in-house clinical ultrasound tomography prototype, Computerized Ultrasound Risk Evaluation (CURE), located at Karmanos Cancer Institute (KCI). Previous publications describe machine operation, image reconstruction, and overall performance in detail.^{39,40} At the time of analysis, the spatial resolution of our transmission measurements were ~ 4 mm and sound speed could be measured to an accuracy of $\sim +/ - 5$ m/s per voxel.³⁹ The slice thickness of the sound speed images is 10 mm.

As an initial proof of concept, an anthropomorphic breast phantom with tissue-equivalent ultrasound characteristics (i.e., density and sound speed) was scanned. The phantom consisted of fat inclusions (density=0.94 g/cc)—with diameters ranging from 6 to 12 mm—embedded in simulated fibroglandular breast tissue (density=1.05 g/cc). Fig. 1 (left) shows the CURE breast phantom and Fig. 1 (right) demonstrates the placement of the phantom in the center of the transducer ring during scanning. In addition, the phantom was scanned, positioned on its base, with a Siemens Somatom Sensation CT scanner (axial slice thickness=1 mm, coronal reconstruction thickness=1 mm, mAs=140, topogram length=256 mm, B31 medium smooth reconstruction kernel). CT is a well-established imaging modality with coronal axis reconstruction available, a characteristic essential for direct comparison to our CURE tomograms. In a clinical setting, MRI would be the preferred modality for comparison due to the American College of Radiology's recent recommendation of its use in breast cancer screening.⁴¹ However, the breast phantom was not MRI-compatible due to its metallic base, and CT served as a suitable alternate despite not typically being employed for breast cancer screening. Furthermore, CT is an x-ray imaging modality and, therefore, more closely related to the comparisons

in vivo with mammography. The phantom was scanned with both CURE and CT at four different timepoints. Beekley CT-Spots® 4.0 mm nonlead pellets were placed on the phantom for consistent experimental setup and orientation between timepoints and modalities. These markers were kept in place for subsequent CT and CURE scans.

The driving hypothesis for this experiment is that if estimated CT scan inclusion volumes (integrated areas) are comparable to those obtained from CURE sound speed tomograms, then a quantitative measure derived from sound speed scans would be a feasible indicator of tissue volume. Note that for this phantom experiment, we are directly comparing integrated areas of simulated fat inclusions segmented from fibroglandular tissue and not calculating USPD. This is meant to evaluate the reproducibility of the sound speed segmentation and the ability to discriminate between fat and fibroglandular simulated tissue.

II.B. Image segmentation and reproducibility

Both CURE sound speed images and corresponding CT scans were imported into the public domain software IMAGEJ (available at: <http://rsb.info.nih.gov/ij/download.html>) for subsequent image analysis.⁴² For each sound speed and CT tomogram, fat inclusions were segmented using a k-means clustering routine previously described.^{38,43} Briefly, k-means clustering employed pixel-based segmentation where each cluster (n) was defined by its centroid in n -dimensional space and established using heuristics.^{29,43,44} User input determined the number of clusters to segment each inclusion. The area for each fat inclusion was calculated on a slice-by-slice basis using IMAGEJ's built-in "analyze particles" function, and an overall volumetric estimate of inclusion volume was calculated by integrating the areas over the entire scanning series. This technique was applied for all four CT and all four CURE scans. To estimate the segmentation variability, the mean integrated area, standard deviation, and standard error were calculated for each fat inclusion in all four scans from both modalities. Finally, the inclusion volume estimations from CURE were compared to those obtained from CT.

II.C. *In vivo* dataset

The patients in this study were recruited from the Walt Comprehensive Breast Center located at KCI, with all imaging procedures being performed under an Institutional Review Board approved protocol, with patient informed consent, and in compliance with the Health Insurance Portability and Accountability Act. The patient population included 93 case sets and provided a variety of breast shapes and densities, with a mean age of 48.2 years (range: 21–85). For the CURE scan, the patients were in the prone position with the whole breast (i.e., ranging from near the chest wall to the nipple region) being imaged.

II.D. *In vivo* ultrasound percent density (USPD)

Because the current protocol for CURE patient recruitment involved patients with masses of approximately 1 cm, these masses were segmented from the sound speed image stack. To identify the extent and location of abnormalities, a radiologist with over 10 years of advanced imaging experience consulted mammograms and conventional ultrasound images. The corresponding CURE reflection images, which emphasize reflecting boundaries and are inherently registered to transmission images as described in previous work,⁴⁰ were also used to localize abnormalities. These regions were then segmented from each sound speed tomogram using a semi-automatic routine and excluded from both the dense and total breast integrated areas to allow a more accurate calculation of volumetric breast density. Approximately 40% of the patients recruited had cysts or complex cysts, which do not currently affect the sound speed images of the breast due to having negligible sound speed differences from breast tissue. For these cases, masses were not segmented from the image stack.

As described in previous work, dense phantom inclusions *in vitro* and dense breasts *in vivo* have demonstrated increased sound speed using our ultrasound tomography clinical prototype.³⁸ To calculate *in vivo* USPD, dense parenchyma regions were segmented from the rest of the breast by implementing the k-means clustering routine previously described in Section II A. Here, the user selected the number of clusters needed to segment elevated sound speed regions from the sound speed tomogram. USPD was calculated in the following manner: if we define a as the first slice near the chest wall, b as the final slice in the image stack at the nipple region, A_D as the dense region of high sound speed, determined using k-means clustering, for that particular slice, and A as the total breast area for that slice, the volumetric ultrasound percent density (USPD) can be calculated using the following equation:

$$\text{USPD}(\%) = \frac{\sum_{n=a}^b A_D}{\sum_{n=a}^b A} \times 100\% .$$

In other words, high sound speed regions were segmented for each tomogram, and the total number of dense voxels was calculated as the integration of high sound speed region areas over the entire breast volume. The total breast area was then estimated for each tomogram, and the voxels were summed over all slices in the breast (~45–75 tomograms). Finally, USPD was calculated as the ratio of high sound speed to total breast integrated areas and converted to a percentage.

II.E. Effect of slice selection

The current acquisition of our data results in a sound speed slice thickness of 10 mm, with 1 mm contiguous slices that yield ~45–75 sound speed slices for each patient. However, the elevation beam of our instrument oversamples each slice by a factor of 5 or more. Therefore, an experiment was conducted to determine the effect of reducing the number of

TABLE I. The BI-RADS compositional category distribution for the patient population.

BI-RADS compositional category	Patient sample (% of population)
1: Fatty (<25%)	11 (12%)
2: Scattered (26%–50%)	60 (65%)
3: Heterogeneous (51%–75%)	16 (17%)
4: Dense (>75%)	6 (7%)

slices used to calculate USPD, without introducing a substantial loss of information. A subsample of 10% of the patient population ($n=10$) of varying breast densities was analyzed using two different approaches: (1) by segmenting every tomogram, and (2) by segmenting every fifth tomogram. A comparison was then made between the two techniques to determine the impact of tomogram reduction on overall USPD.

II.F. BI-RADS Category analysis

As an independent evaluation of our approach, we compared the USPD to the current standard of care for breast density analysis (i.e., BI-RADS categories). A board-certified radiologist with over 10 years of mammography experience examined the mammograms corresponding closest to the CURE exam date, and assigned each patient into a BI-RADS compositional category of: (1) almost entirely fat (<25% glandular), (2) scattered (25%–50% glandular), (3) heterogeneously dense (51%–75% glandular), and (4) extremely dense (>75% glandular). The resulting population distribution is shown in Table I.

A one-way ANOVA tested for significant differences in mean USPD between BI-RADS categories and a Spearman correlation coefficient was calculated to determine the association between the two variables.

II.G. Quantitative breast density analysis

To determine a more quantitative comparison of MPD, mammograms acquired closest to the CURE exam date (typically within 1 month) in the craniocaudal (CC) and mediolateral (MLO) projections were digitized with a Vidar VXR-16 Dosimetry Pro digitizer using a TWAIN interface (version 5.2.1) with the following parameters: logarithmic translation table, 71 dpi resolution, and an 8-bit depth. Pre-

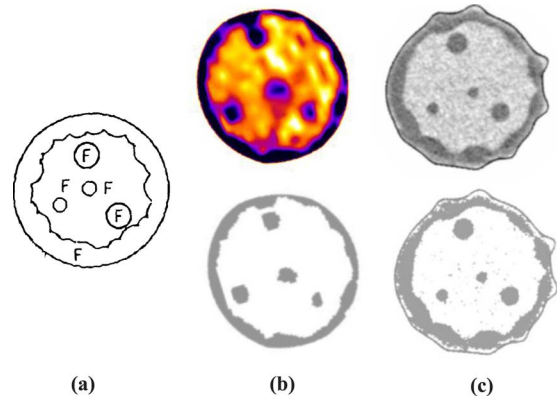


FIG. 2. (a) Phantom cross section as provided by the manufacturer, where F denotes “fat” and the remainder is fibroglandular tissue (Ref. 46), (b) a sound speed tomogram (top) and the resulting k-means clustering segmentation of the inclusions from the sound speed scan (bottom), and (c) a CT tomogram (top) with its corresponding segmentation (bottom).

vious work has shown this resolution and depth to be sufficient for MPD calculation,²⁹ particularly because as a ratio, MPD is known to be a coarse measure.⁴⁵ A segmentation routine for breast density evaluation, described in detail elsewhere^{29,38} was then employed. Finally, we compared the USPD to calculated MPD for both CC and MLO views, and corresponding associations between the variables were determined.

III. RESULTS

III.A. Phantom analysis

Figure 2(a) shows the phantom cross section as provided by the manufacturer at time of phantom construction, where F denotes “fat” and the remainder is fibroglandular tissue.⁴⁶ Shown also is a sound speed tomogram (b, top) and resulting k-means clustering inclusion segmentation (b, bottom), and finally, the corresponding CT tomogram (c, top) and its corresponding segmentation (c, bottom). The fat inclusions and subcutaneous fat layer were readily distinguishable from the surrounding fibroglandular tissue in both the CT scan and CURE sound speed tomogram. Furthermore, the k-means clustering routine used in segmentation clearly demarcated the boundary between each fat inclusion and surrounding fibroglandular tissue. The mean integrated area and descriptive statistics for the four CT and CURE sound speed scans

TABLE II. Mean integrated areas and statistics for each phantom component segmented from four different CURE sound speed and CT scans.

Phantom component (clock position)	CT inclusion		Sound speed inclusion	
	Area ± Standard deviation (pixel ²)	Standard error	Area ± Standard deviation (pixel ²)	Standard error
Large fat (12:00)	7517 ± 123	61	6868 ± 161	80
Large fat (4:00)	7625 ± 134	67	7139 ± 629	314
Small fat (center)	1136 ± 44	22	2091 ± 190	95
Small fat (7:00)	1019 ± 24	12	1983 ± 146	73

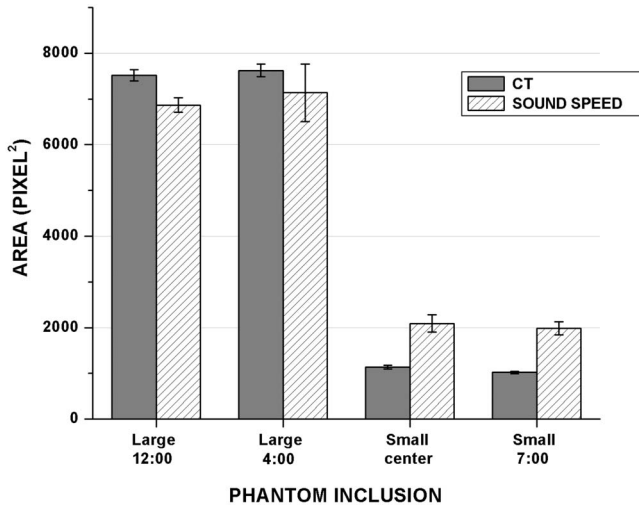


FIG. 3. A comparison of the integrated area for the segmented CT scan and the segmented sound speed scan the CURE phantom. The sound speed scans underestimated both large fat inclusions, which may be due to partial volume effects.

are summarized in Table II. In order to directly compare the sound speed areas to the CT areas, the sound speed images (440 × 440 pixel²), were scaled to have the same size as the CT scans (512 × 512 pixel²).

Figure 3 better illustrates the comparison between the mean integrated areas for each CT and sound speed scan inclusion. The error bars indicate one standard deviation of the mean. The reproducibility of segmentation analysis for consecutive CT and CURE scans was also assessed. Overall, the average standard deviation for CT integrated areas was 2.4% of the mean (range: 1.6%–3.9%) and 6.9% of the mean (range: 2.3%–9.1%) for sound speed.

III.B. In vivo results

III.B.1. Segmentation

Figure 4 (left) shows a typical patient sound speed tomogram, with varying sound speed patterns ranging from ~1400 to ~1550 m/s (shown in the scale). Applying k-means clustering segmentation to the sound speed tomogram with four clusters yields the segmentation shown in Fig. 4 (right), with the scale indicating the number of clusters. This example illustrates that high sound speed regions are readily discernible from the rest of the breast by implementing the segmentation routine.

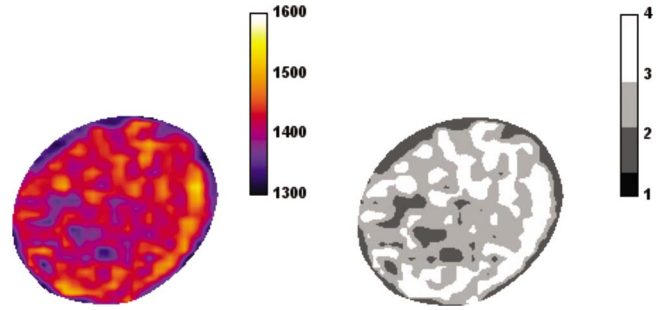


FIG. 4. (Left) Sound speed tomogram (scale is sound speed in m/s) and (right) k-means clustered sound speed image (scale is cluster number). Note the high sound speed regions are clearly demarcated by using the clustering technique.

III.B.2. Tomogram reduction

For the patient data, an experiment was performed to determine the effects of using every fifth sound speed slice as opposed to using every slice in the USPD analysis. Figure 5 shows the correlation of the USPD results for every slice compared to every fifth slice. A strong positive association (Pearson $r=0.994$, $p<0.001$) was observed between the USPD for segmenting every slice and every fifth slice, with a standard error of the estimate of 1.93. A linear fit through the data points yielded the following equation: $y=1.05x-2.59$, where y indicates the USPD using every fifth slice and x is the calculated USPD using every single slice.

III.B.3. Correlation with BI-RADS categories

As a comparison to the current standard of care for breast density analysis, we compared the USPD using every fifth slice to BI-RADS categories, and the results are summarized by the boxplot in Fig. 6. In general, a strong positive association was observed between USPD and BI-RADS category (Spearman $\rho=0.69$, $p<0.001$). A one-way analysis of variance revealed that a significant difference existed between the mean USPD among BI-RADS categories ($p<0.01$). Further posthoc analyses using the Scheffé criterion indicated that significant differences in mean USPD were observed between each BI-RADS category ($\alpha=0.05$). Table III below best summarizes the descriptive statistics of the USPD calculation for each BI-RADS category.

Notably, the mean difference in USPD between fatty breasted patients (BI-RADS 1) and dense breasted patients (BI-RADS 4) was approximately 39.5% (standard error

TABLE III. The mean USPD, standard deviation of the mean, and standard error for each BI-RADS category.

BI-RADS category	Mean USPD ± Standard deviation (%)	Standard error
1	20.48 ± 6.75	2.04
2	27.02 ± 6.62	0.85
3	40.62 ± 7.55	1.89
4	60.03 ± 7.65	3.12
Total	30.72 ± 11.83	1.22

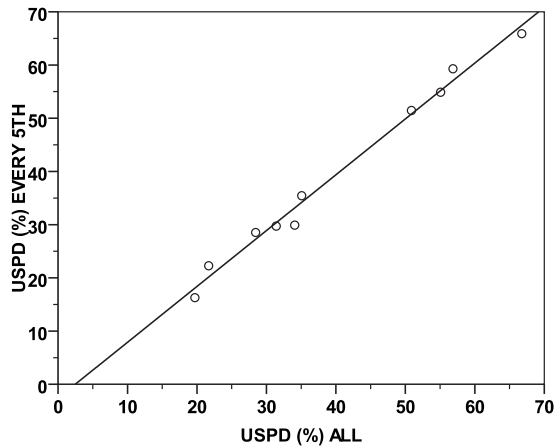


FIG. 5. A comparison of using every slice and every fifth slice for the USPDP calculation *in vivo*. The strong correlation (Pearson $r=0.994$) between techniques justified the reduction of slices used in the USPDP analysis.

=3.5%). Comparing USPDP to the current standard of care is important to determining the clinical relevance of our technique.

III.B.4. Correlation with MPD

To further validate our approach, we compared USPDP to calculated mammographic percent density for both CC and MLO mammographic views. Figures 7(a) and 7(c) show the data for CC and MLO views, respectively. Because comparisons were made between volumetric (USPD) and area (MPD) measures, curve fitting was used to take this into account in a manner similar to what has been previously applied to MRI breast density analysis.³⁶ Briefly, as Wei *et al.* described, if we assume a simplified case with a dense tissue spherical volume embedded in a spherical shell of fatty tissue, the volume (i.e., USPDP) would be proportional to the projected area (MPD) to the 3/2 power. Figures 7(b)

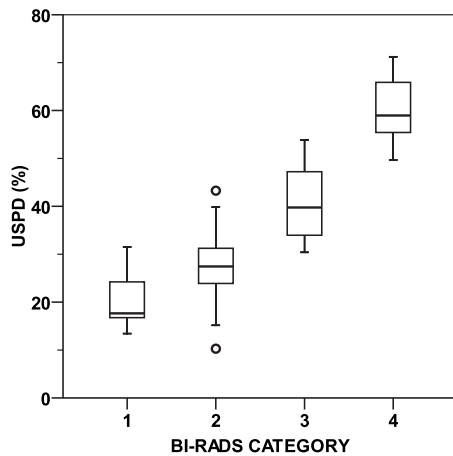


FIG. 6. Boxplot showing the strong correlation [Spearman $\rho=0.69$ ($p < 0.001$)] between the USPDP for 93 patients categorized by BI-RADS compositional category. The differences between all BI-RADS categories were found to be significant using a one-way ANOVA and Scheffé posthoc analysis, demonstrating the agreement of the USPDP technique with the current standard of care.

TABLE IV. An analysis of the relationship between volumetric ultrasound percent density (y) from CURE sound speed tomograms and mammographic percent density (x) for CC and MLO views obtained by a volume to area comparison model.

Mathematical equation	Correlation coefficient (r^2)
Cranio-caudal view $y = 15.849 + 0.072x^{3/2}$	0.746
Mediolateral view $y = 14.70 + 0.063x^{3/2}$	0.588

and 7(d) show the results with this 3/2 fit applied. Moderate to strong positive correlations were observed between percent area and percent volume for both CC and MLO views ($r^2=0.75$ and 0.59 , respectively). Table IV summarizes the results.

IV. DISCUSSION

We sought to demonstrate the feasibility of employing ultrasound tomography to estimate volumetric breast density. As an initial proof of concept, we imaged an anthropomorphic breast phantom with both CURE and CT to determine if estimated phantom inclusion volumes (integrated areas) were comparable between the two modalities. Overall, close agreement was observed for the large fat inclusions (diameter=12 mm), whereas the sound speed scan overestimated the small fat inclusions with the diameter of 6 mm. Using the current reconstruction algorithms, the resolution of the prototype sound speed images is ~ 4 mm. As a result, partial averaging of the sound speed measurements was observed between the smaller (6 mm) inclusions and adjacent fibroglandular tissue. As evident in Table II, the standard deviations and standard errors for the smaller fat inclusions were clearly higher for sound speed than for CT scan segmentation. Similarly, the standard deviation of the sound speed integrated areas was higher at $\sim 7\%$ of the mean, while for CT it was $\sim 2\%$. Efforts are currently underway to employ algorithms using bent-ray approximations or waveform tomography, which are expected to improve sound speed resolution, and consequently, improve volumetric estimations.⁴⁷ Despite the current limitations in sound speed resolution, these *in vitro* results were encouraging, and further analysis was conducted to establish the feasibility of implementing this technique *in vivo*.

First, the strong association (Pearson $r=0.994$, $p < 0.001$) found between segmenting the sound speed stacks for every fifth slice and every slice in 10% of our patient population indicated that using every fifth slice did not strongly influence the calculation of USPDP for this subset of data. Therefore, this justified using every fifth slice in subsequent analyses for a reduction in workload. Because a single patient sound speed stack can contain up to 75 sound speed tomograms, using every fifth slice made the sample of ~ 100 patients more manageable. Another reason we could legiti-

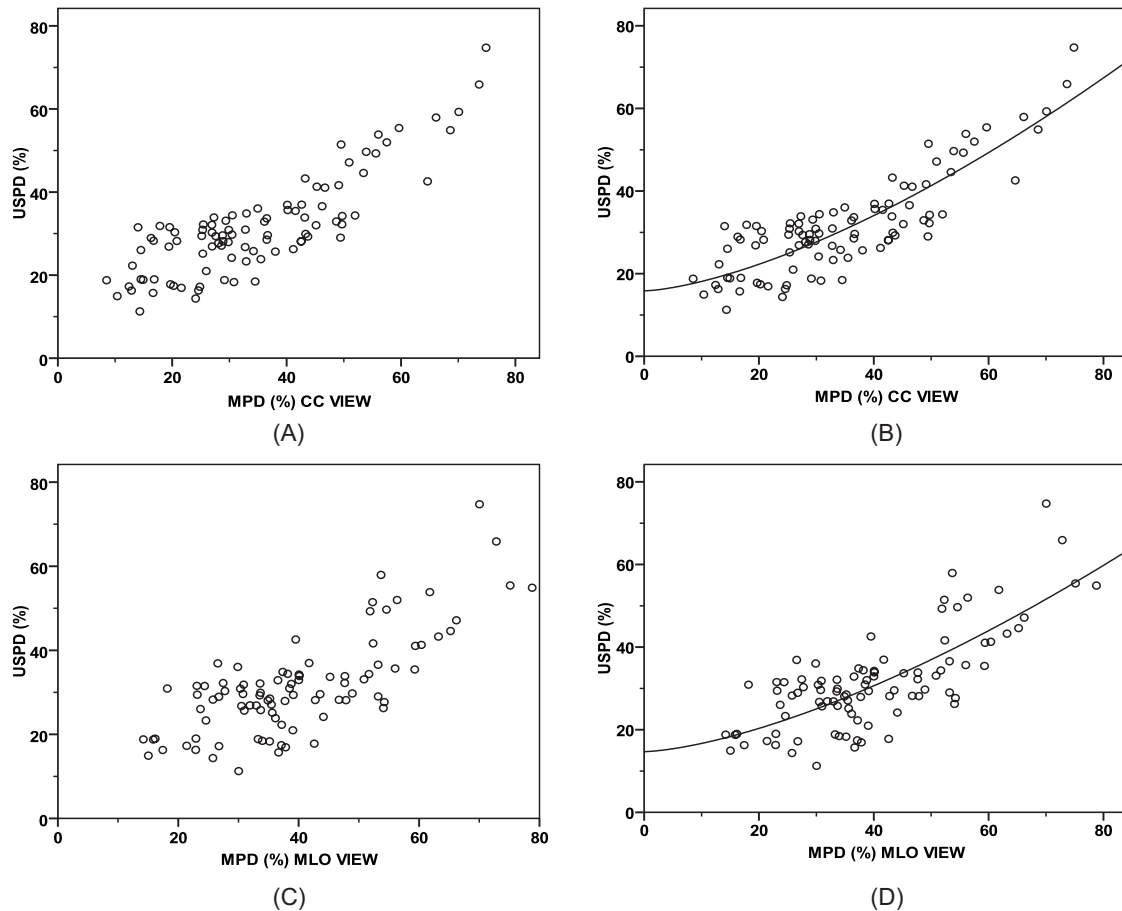


FIG. 7. A comparison of the ultrasound percent density (USPD) for every fifth sound speed tomogram and quantitative mammographic percent density (MPD) for 93 patients. (a) Observed data for the CC view, (b) volume to area fit, Pearson $r=0.75$, (c) observed data for the MLO view, (d) volume to area fit, Pearson $r=0.59$.

mately use every fifth slice is the fact that the elevation beam of our instrument was oversampled by a factor of 5 or more, thereby ensuring little loss of information.

As an independent evaluation of our USPDP approach, we arranged USPDP according to BI-RADS category. In general, a strong increase in USPDP was observed with increasing BI-RADS breast density category. Statistically significant differences in mean USPDP were found between each of the four BI-RADS breast density categories. Most notably, the difference in USPDP between BI-RADS 1 (fatty) and BI-RADS 4 (dense) was $\sim 40\%$. This is a critical result because it showed that there was a substantial change in USPDP between women in the highest breast cancer risk category compared to those in the lowest. The magnitude of difference between the USPDP for fatty versus dense-breasted patients indicates the potential value in employing USPDP to identify women with dense breasts who are at increased breast cancer risk.

By definition, the BI-RADS categories are set to a coarse scale, thus a wide range of USPDP values for each breast density category was observed. As expected, this was most apparent for BI-RADS category 2 patients where $\sim 60\%$ of our patient population was included. Despite this limitation, evaluating USPDP with the current standard of care was necessary to determine the clinical usefulness of our approach,

and our results were strongly correlated. To more quantitatively evaluate USPDP, we made a direct comparison of USPDP with calculated MPDP.

Using a volume to area model to fit the USPDP to MPDP data, moderate to strong positive correlations were observed for both CC and MLO views. A stronger association was observed between USPDP and CC MPDP view compared to that of the MLO view. This is most likely due to the reduction of sound speed tomograms, where every fifth sound speed tomogram was used in the USPDP analysis (i.e., starting at slice 5, 10, 15, etc.). As a result, the chest wall region was not included in the calculation of USPDP.

A distinct advantage of our approach over using mammography for breast density estimation is that the stacked tomographic information provides a volumetric estimation of breast density covering the entire breast. Other researchers have estimated volumetric breast density through the evaluation of whole-breast MRI sequences,^{36,37} although this method is currently not practical because of high cost and long exam time required for imaging. The usefulness of calibrating screen-film images with step wedges has also been investigated.³² However, this approach is not ideal because it does not account for variations in breast thickness at the peripheral tissue regions, while also utilizing ionizing radia-

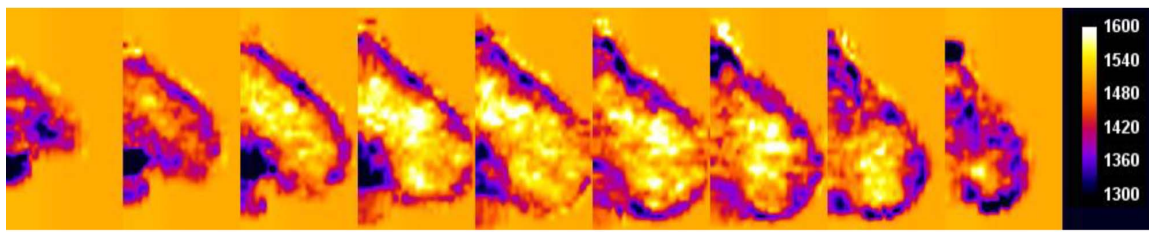


FIG. 8. Sound speed images of a BI-RADS category 3 (heterogeneous) breast reconstructed in the sagittal plane (left to right), with every fifth slice shown (legend shows sound speed in m/s). Being able to investigate different cross sections of the breast eliminates the effects that surrounding tissue may have on decreasing image contrast, and allows a more ready comparison to conventional mammography.

tion. Furthermore, many women are reluctant to get mammograms due to the pain and anxiety associated with breast compression.^{48–50} Our method of imaging does not require compression; the patients we have imaged thus far have responded favorably about the comfort of the scan. Further, utilizing a method that does not require compression allows the distribution of tissue inside the breast to remain in a more natural state during the scanning procedure.

Preliminary work has also been suggested to evaluate breast density using dedicated breast CT,⁵¹ and tomosynthesis mammography devices, which are now available that allow multiple sequential area estimates.⁵² However, employing ultrasound for breast density evaluation offers the unique advantage of taking repeated measurements without ionizing radiation concerns. Introducing a means of temporal breast density monitoring would be useful to track breast density changes in response to chemopreventative agents, hormonal therapies, or radiation therapy. Overall, calculating USPD through sound speed segmentation in a manner analogous to MPD provides estimates of the volume of dense tissue as opposed to the projected area. It is expected that breast cancer risk would be more strongly associated with the volumetric amount of dense tissue, which we have shown to be a feasible measurement using transmission ultrasound tomography.

Some shortcomings in our current study include: the coarse scale used for BI-RADS category, limited sample size with the majority of our sample in the intermediate breast density categories, having only one set of scans per patient, and the current limited resolution of the CURE sound speed images. However, most of these issues can be addressed in a larger clinical trial that controls for menstrual cycle in premenopausal women and allows repeated measurements to determine inpatient variability. Current efforts are underway to evaluate the use of bent-ray reconstructions to improve sound speed resolution, which has already shown to be promising in improving the image resolution to less than 2 mm.⁴⁷ Another limitation is that the segmentation methodology currently employed is semiautomatic and relies on user input to determine the number of clusters for segmentation. While a completely automated USPD segmentation would be preferred, most assessments of breast density involve user interaction (i.e., thresholding^{3,53} or subjective assessment²⁷). Future studies could involve efforts to automate segmentation, possibly similar to a computer-aided

classification system where pattern recognition could be utilized. Our group is currently investigating the use of automated procedures and we see this is a natural endpoint of this line of investigation.

A comparison between CT and mammography revealed that contrast in breast imaging is strongly related to the presence of overlying tissue obscuring structures.⁵¹ Clearly, this is a significant disadvantage for mammography, which collapses all of the volumetric information into two dimensions. Because our ultrasound tomography technique allows us to assess cross-sectional tomograms, we are able to evaluate the distribution of fatty and glandular tissue on a planar level, an option currently not possible with mammography. Furthermore, because of our volumetric data acquisition, we can reslice coronal sound speed tomograms into different planes using IMAGEJ, as demonstrated for a patient's breast in Fig. 8. Here, a BI-RADS category 3 (heterogeneous) breast was reconstructed in the sagittal plane (left to right), and every fifth slice is shown, with the breast sound speed (m/s) indicated in the legend. Being able to investigate different cross sections of the breast eliminates the effects that surrounding tissue may have on decreasing image contrast. Furthermore, by performing an average intensity summation of multiple tomograms, creating an ultrasound tomography "mammogram" is possible, allowing a more direct comparison to conventional mammographic views. This may have additional clinical utility in that it relates our sound speed images to the mammographic views that are the current standard of care in breast cancer screening. Further segmentation of high sound speed regions from these different views is also possible, without additional ionizing radiation risk concerns. Future work will involve investigating image fusion with mammography and evaluating temporal changes in the breast composition. Further studies will also be conducted to combine acoustic parameters including USPD, as presented here, and global sound speed measurements, as described previously.³⁸ When used in concert, these parameters may demonstrate better discriminating power in the identification of women with dense breasts.

V. CONCLUSION

The feasibility and accuracy of using USPD to evaluate breast density has been established through both a phantom study and *in vivo* investigation, suggesting that the USPD

methods described in this work may be implemented for breast density evaluation. The association of USPD with mammographic percent density has been demonstrated qualitatively, using BI-RADS criteria and quantitatively, via digitization and semiautomatic segmentation of craniocaudal and mediolateral oblique mammograms. A positive association between BI-RADS category and USPD was demonstrated [Spearman $\rho=0.69$ ($p<0.001$)]. Furthermore, comparing USPD to calculated mammographic density yielded moderate to strong positive associations for CC and MLO views ($r^2=0.75$ and 0.59 , respectively). These results support the hypothesis that utilizing USPD as an analog to mammographic breast density is feasible. Overall, USPD has the potential to provide volumetric whole-breast analysis of breast density, which may better elucidate the relationship between breast density and breast cancer risk.

Using ultrasound tomography for breast density evaluation is advantageous for a few reasons: it is noninvasive, nonionizing, and calculations are performed on an uncompressed breast. By accurately identifying women who are at a higher breast cancer risk due in part to increased breast density, our approach would enable preventive measures that have the potential to monitor a quantitative variable that may correspond to eventual reduction in breast cancer incidence.

ACKNOWLEDGMENTS

We would like to thank Olsi Rama for assistance in data processing and Lisa Bey-Knight for her help with patient recruitment. Furthermore, we wish to thank the staff of the Alexander J. Walt Comprehensive Breast Cancer Center at the Karmanos Cancer Institute for their generous assistance with patient management.

^{a)} Author to whom correspondence should be addressed. Electronic mail: Carri.Glide-Hurst@beaumont.edu; Telephone: 248-551-7479.

¹N. F. Boyd, J. W. Byng, R. A. Jong, E. K. Fishell, L. E. Little, A. B. Miller, G. A. Lockwood, D. L. Tritchler, and M. J. Yaffe, "Quantitative classification of mammographic densities and breast cancer risk: Results from the Canadian National Breast Screening Study," *J. Natl. Cancer Inst.* **87**, 670–675 (1995).

²N. F. Boyd, G. S. Dite, J. Stone, A. Gunasekara, D. R. English, M. R. McCredie, G. G. Giles, D. Tritchler, A. Chiarelli, M. J. Yaffe, and J. L. Hopper, "Heritability of mammographic density, a risk factor for breast cancer," *N. Engl. J. Med.* **347**, 886–894 (2002).

³M. J. Yaffe, N. F. Boyd, J. W. Byng, R. A. Jong, E. Fishell, G. A. Lockwood, L. E. Little, and D. L. Tritchler, "Breast cancer risk and measured mammographic density," *Eur. J. Cancer Prev.* **7 Suppl 1**, S47–55 (1998).

⁴J. N. Wolfe, A. F. Saftlas, and M. Salane, "Mammographic parenchymal patterns and quantitative evaluation of mammographic densities: A case-control study," *AJR, Am. J. Roentgenol.* **148**, 1087–1092 (1987).

⁵N. F. Boyd, H. Guo, L. J. Martin, L. Sun, J. Stone, E. Fishell, R. A. Jong, G. Hislop, A. Chiarelli, S. Minkin, and M. J. Yaffe, "Mammographic density and the risk and detection of breast cancer," *N. Engl. J. Med.* **356**, 227–236 (2007).

⁶W. E. Barlow, E. White, R. Ballard-Barbash, P. M. Vacek, L. Titus-Ernstoff, P. A. Carney, J. A. Tice, D. S. Buist, B. M. Geller, R. Rosenberg, B. C. Yankaskas, and K. Kerlikowske, "Prospective breast cancer risk prediction model for women undergoing screening mammography," *J. Natl. Cancer Inst.* **98**, 1204–1214 (2006).

⁷N. F. Boyd, G. A. Lockwood, J. W. Byng, D. L. Tritchler, and M. J. Yaffe, "Mammographic densities and breast cancer risk," *Cancer Epidemiol. Biomarkers Prev.* **7**, 1133–1144 (1998).

⁸J. A. Harvey and V. E. Bovbjerg, "Quantitative assessment of mammo-

graphic breast density: Relationship with breast cancer risk," *Radiology* **230**, 29–41 (2004).

⁹C. Byrne, C. Schairer, J. Wolfe, N. Parekh, M. Salane, L. A. Brinton, R. Hoover, and R. Haile, "Mammographic features and breast cancer risk: Effects with time, age, and menopause status," *J. Natl. Cancer Inst.* **87**, 1622–1629 (1995).

¹⁰K. E. Malone, J. R. Daling, D. R. Doody, L. Hsu, L. Bernstein, R. J. Coates, P. A. Marchbanks, M. S. Simon, J. A. McDonald, S. A. Norman, B. L. Strom, R. T. Burkman, G. Ursin, D. Deapen, L. K. Weiss, S. Folger, J. J. Madeoy, D. M. Friedrichsen, N. M. Suter, M. C. Humphrey, R. Spirtas, and E. A. Ostrander, "Prevalence and predictors of BRCA1 and BRCA2 mutations in a population-based study of breast cancer in white and black American women ages 35 to 64 years," *Cancer Res.* **66**, 8297–8308 (2006).

¹¹B. Newman, H. Mu, L. M. Butler, R. C. Millikan, P. G. Moorman, and M. C. King, "Frequency of breast cancer attributable to BRCA1 in a population-based series of American women," *JAMA, J. Am. Med. Assoc.* **279**, 915–921 (1998).

¹²H. Anton-Culver, P. F. Cohen, M. E. Gildea, and A. Ziogas, "Characteristics of BRCA1 mutations in a population-based case series of breast and ovarian cancer," *Eur. J. Cancer* **36**, 1200–1208 (2000).

¹³C. B. Begg, R. W. Haile, A. Borg, K. E. Malone, P. Concannon, D. C. Thomas, B. Langholz, L. Bernstein, J. H. Olsen, C. F. Lynch, H. Anton-Culver, M. Capanu, X. Liang, A. J. Hummer, C. Sima, and J. L. Bernstein, "Variation of breast cancer risk among BRCA1/2 carriers," *JAMA, J. Am. Med. Assoc.* **299**, 194–201 (2008).

¹⁴N. F. Boyd, L. J. Martin, Q. Li, L. Sun, A. M. Chiarelli, G. Hislop, M. J. Yaffe, and S. Minkin, "Mammographic density as a surrogate marker for the effects of hormone therapy on risk of breast cancer," *Cancer Epidemiol. Biomarkers Prev.* **15**, 961–966 (2006).

¹⁵N. F. Boyd, J. M. Rommens, K. Vogt, V. Lee, J. L. Hopper, M. J. Yaffe, and A. D. Paterson, "Mammographic breast density as an intermediate phenotype for breast cancer," *Lancet Oncol.* **6**, 798–808 (2005).

¹⁶N. F. Boyd, L. J. Martin, J. Stone, C. Greenberg, S. Minkin, and M. J. Yaffe, "Mammographic densities as a marker of human breast cancer risk and their use in chemoprevention," *Curr. Oncol. Rep.* **3**, 314–321 (2001).

¹⁷C. Atkinson, R. M. Warren, E. Sala, M. Dowsett, A. M. Dunning, C. S. Healey, S. Runswick, N. E. Day, and S. A. Bingham, "Red-clover-derived isoflavones and mammographic breast density: A double-blind, randomized, placebo-controlled trial," *Breast Cancer Res.* **6**, R170–179 (2004).

¹⁸J. Brisson, B. Brisson, G. Coté, E. Maunsell, S. Bérubé, and J. Robert, "Tamoxifen and mammographic breast densities," *Cancer Epidemiol. Biomarkers Prev.* **9**, 911–915 (2000).

¹⁹J. A. Harvey, V. E. Bovbjerg, M. E. Smolkin, M. B. Williams, and G. R. Petroni, "Evaluating hormone therapy-associated increases in breast density comparison between reported and simultaneous assignment of BI-RADS categories, visual assessment, and quantitative analysis 1," *Acad. Radiol.* **12**, 853–862 (2005).

²⁰C. M. Rutter, M. T. Mandelson, M. B. Laya, D. J. Seger, and S. Taplin, "Changes in breast density associated with initiation, discontinuation, and continuing use of hormone replacement therapy," *JAMA, J. Am. Med. Assoc.* **285**, 171–176 (2001).

²¹E. E. Sterns and B. Zee, "Mammographic density changes in perimenopausal and postmenopausal women: Is effect of hormone replacement therapy predictable?," *Breast Cancer Res. Treat.* **59**, 125–132 (2000).

²²C. M. Vachon, T. A. Sellers, R. A. Vierkant, E. F. Wu, and K. R. Brandt, "Case-control study of increased mammographic breast density response to hormone replacement therapy," *Cancer Epidemiol. Biomarkers Prev.* **11**, 1382–1388 (2002).

²³C. K. Chow, D. Venzon, E. C. Jones, A. Premkumar, J. O'Shaughnessy, and J. Zujewski, "Effect of tamoxifen on mammographic density," *Cancer Epidemiol. Biomarkers Prev.* **9**, 917–921 (2000).

²⁴G. Maskarinec and L. Meng, "An investigation of soy intake and mammographic characteristics in Hawaii," *Breast Cancer Res.* **3**, 134–141 (2001).

²⁵A. H. Wu, P. Wan, J. Hankin, C. C. Tseng, M. C. Yu, and M. C. Pike, "Adolescent and adult soy intake and risk of breast cancer in Asian-Americans," *Carcinogenesis* **23**, 1491–1496 (2002).

²⁶X. O. Shu, F. Jin, Q. Dai, W. Wen, J. D. Potter, L. H. Kushi, Z. Ruan, Y. T. Gao, and W. Zheng, "Soyfood intake during adolescence and subsequent risk of breast cancer among Chinese women," *Cancer Epidemiol. Biomarkers Prev.* **10**, 483–488 (2001).

²⁷S. Ciatto, N. Houssami, A. Apruzzese, E. Bassetti, B. Brancato, F.

- Carozzi, S. Catarzi, M. P. Lamberini, G. Marcelli, R. Pellizzoni, B. Pesce, G. Risso, F. Russo, and A. Scorsolini, "Categorizing breast mammographic density: Intra- and interobserver reproducibility of BI-RADS density categories," *Breast J.* **14**, 269–275 (2005).
- ²⁸W. A. Berg, C. Campassi, P. Langenberg, and M. J. Sexton, "Breast imaging reporting and data system: Inter- and intraobserver variability in feature analysis and final assessment," *AJR, Am. J. Roentgenol.* **174**, 1769–1777 (2000).
- ²⁹C. K. Glide-Hurst, N. Duric, and P. Littrup, "A new method for quantitative analysis of mammographic density," *Med. Phys.* **34**, 4491–4498 (2007).
- ³⁰C. Zhou, H. P. Chan, N. Petrick, M. A. Helvie, M. M. Goodsitt, B. Sahiner, and L. M. Hadjiiski, "Computerized image analysis: Estimation of breast density on mammograms," *Med. Phys.* **28**, 1056–1069 (2001).
- ³¹J. W. Byng, N. F. Boyd, E. Fishell, R. A. Jong, and M. J. Yaffe, "The quantitative analysis of mammographic densities," *Phys. Med. Biol.* **39**, 1629–1638 (1994).
- ³²O. Pawluczyk, B. J. Augustine, M. J. Yaffe, D. Rico, J. Yang, G. E. Mawdsley, and N. F. Boyd, "A volumetric method for estimation of breast density on digitized screen-film mammograms," *Med. Phys.* **30**, 352–364 (2003).
- ³³J. A. Harvey, "Quantitative assessment of percent breast density: Analog versus digital acquisition," *Technol. Cancer Res. Treat.* **3**, 611–616 (2004).
- ³⁴M. Jeffreys, R. Warren, R. Highnam, and G. D. Smith, "Initial experiences of using an automated volumetric measure of breast density: The standard mammogram form," *Br. J. Radiol.* **79**, 378–382 (2006).
- ³⁵S. van Engeland, P. R. Snoeren, H. Huisman, C. Boetes, and N. Karssemeijer, "Volumetric breast density estimation from full-field digital mammograms," *IEEE Trans. Med. Imaging* **25**, 273–282 (2006).
- ³⁶J. Wei, H. P. Chan, M. A. Helvie, M. A. Roubidoux, B. Sahiner, L. M. Hadjiiski, C. Zhou, S. Paquerault, T. Chenevert, and M. M. Goodsitt, "Correlation between mammographic density and volumetric fibroglandular tissue estimated on breast MR images," *Med. Phys.* **31**, 933–942 (2004).
- ³⁷R. C. Boston, M. D. Schnall, S. A. Englander, J. R. Landis, and P. J. Moate, "Estimation of the content of fat and parenchyma in breast tissue using MRI T1 histograms and phantoms," *Magn. Reson. Imaging* **23**, 591–599 (2005).
- ³⁸C. Glide, N. Duric, and P. Littrup, "Novel approach to evaluating breast density utilizing ultrasound tomography," *Med. Phys.* **34**, 744–753 (2007).
- ³⁹N. Duric, P. Littrup, A. Babkin, D. Chambers, S. Azevedo, R. Pevzner, M. Tokarev, E. Holsapple, O. Rama, and R. Duncan, "Development of ultrasound tomography for breast imaging: Technical assessment," *Med. Phys.* **32**, 1375–1386 (2005).
- ⁴⁰N. Duric, P. Littrup, L. Poulou, A. Babkin, R. Pevzner, E. Holsapple, O. Rama, and C. Glide, "Detection of breast cancer with ultrasound tomography: First results with the Computed Ultrasound Risk Evaluation (CURE) prototype," *Med. Phys.* **34**, 773–785 (2007).
- ⁴¹D. Saslow, C. Boetes, W. Burke, S. Harms, M. O. Leach, C. D. Lehman, E. Morris, E. Pisano, M. Schnall, S. Sener, R. A. Smith, E. Warner, M. Yaffe, K. S. Andrews, and C. A. Russell, "American cancer society guidelines for breast screening with MRI as an adjunct to mammography," *Ca-Cancer J. Clin.* **57**, 75–89 (2007).
- ⁴²W. S. Rasband, "ImageJ," (National Institutes of Health, Bethesda, Maryland, USA, 1997).
- ⁴³SourceForge.net, "IJ Plugins: Clustering."
- ⁴⁴A. K. Jain and R. C. Dubes, *Algorithms for Clustering Data* (Prentice Hall, Englewood Cliffs, New Jersey, 1988).
- ⁴⁵J. W. Byng, N. F. Boyd, E. Fishell, R. A. Jong, and M. J. Yaffe, "Automated analysis of mammographic densities," *Phys. Med. Biol.* **41**, 909–923 (1996).
- ⁴⁶E. Madsen (personal communication, 2007).
- ⁴⁷C. Li, N. Duric, and Y. Huang, "Calibration of bent-ray ultrasound tomography and its application to breast cancer detection and diagnosis," *Med. Phys.* **34**, 2645 (2007).
- ⁴⁸A. R. Aro, P. Absetz-Ylostalo, T. Eerola, M. Pamilo, and J. Lonnqvist, "Pain and discomfort during mammography," (1996), pp. 1674–1679.
- ⁴⁹S. Kashikar-Zuck, F. J. Keefe, P. Kornguth, P. Beaupre, A. Holzberg, and D. DeLong, "Pain coping and the pain experience during mammography: A preliminary study," (1997), pp. 165–172.
- ⁵⁰P. J. Kornguth, F. J. Keefe, and M. R. Conaway, "Pain during mammography: Characteristics and relationship to demographic and medical variables," (1996), pp. 187–194.
- ⁵¹J. M. Boone and K. K. Lindfors, "Breast CT: Potential for breast cancer screening and diagnosis," *Future Oncol.* **2**, 351–356 (2006).
- ⁵²H. P. Chan, J. Wei, B. Sahiner, E. A. Rafferty, T. Wu, M. A. Roubidoux, R. H. Moore, D. B. Kopans, L. M. Hadjiiski, and M. A. Helvie, "Computer-aided detection system for breast masses on digital tomosynthesis mammograms: Preliminary experience," *Radiology* **237**, 1075–1080 (2005).
- ⁵³N. Jamal, K. H. Ng, L. M. Looi, D. McLean, A. Zulfikar, S. P. Tan, W. F. Liew, A. Shantini, and S. Ranganathan, "Quantitative assessment of breast density from digitized mammograms into Tabar's patterns," *Phys. Med. Biol.* **51**, 5843–5857 (2006).